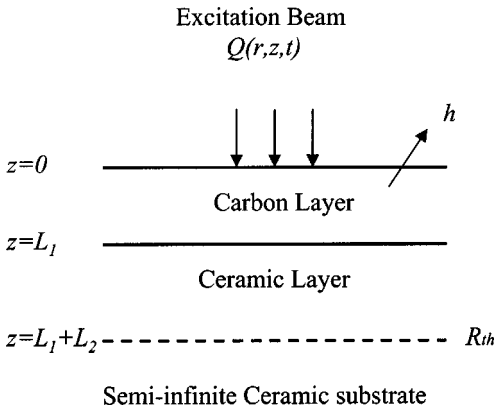

FIG. 1. Three-layered sample structure for the theoretical model.

and infrared emission, a ceramic under layer with thickness comparable to the mean size of the ceramic grains, and a semi-infinite ceramic substrate. The pump beam is totally absorbed by the carbon layer. There exists a thermal boundary resistance between the ceramic under layer and the ceramic substrate. A continuously modulated laser beam illuminates the sample surface perpendicularly. Modulated heat (a thermal wave) is created in the carbon layer and conducts into the ceramic layer and substrate. In the case of high infrared emission/absorption coefficient, the PTR signal is directly proportional to the temperature oscillation of the surface of the carbon layer. The resulting surface temperature rise is[19]

$$\Delta T(z=0,\omega)=\frac{1}{2}\int_0^\infty \delta d\,\delta J_0(\delta r)\{[A_1(\delta)+B_1(\delta)+E(\delta)]\times\exp(j\omega t)+\text{c.c.}\} \tag{1}$$

with

$$A_1(\delta)=-(g_1+s_1)(p_2+g_2)E(\delta)/H(\delta), \tag{2}$$

$$B_1(\delta)=-(g_1+s_1)(p_2-g_2)\exp(-2\beta_1 L_1)E(\delta)/H(\delta), \tag{3}$$

$$E(\delta)=\frac{\alpha(1-R)P}{2\pi K_1}\frac{\exp(-\delta^2 a^2/4)}{\beta_1^2-\alpha^2}, \tag{4}$$

where

$$H(\delta)=(1+g_1)[p_2+g_2]-(1-g_1)[p_2-g_2]\times\exp(-2\beta_1 L_1), \tag{5}$$

$$g_1=h/K_1\beta_1, \tag{6}$$

$$s_1=\alpha/\beta_1, \tag{7}$$

$$g_i=K_i\beta_i/K_1\beta_1 \quad (i=2,3), \tag{8}$$

$$p_2=\frac{1+\mu_2}{1-\mu_2}, \tag{9}$$

$$\mu_2=\frac{g_2-g_3(1-b)}{g_2+g_3(1+b)}\exp(-2\beta_2 L_2), \tag{10}$$

$$b=K_2\beta_2 R_{\text{th}}, \tag{11}$$

$$\beta_i^2=\delta^2+j\omega/D_i \quad (i=1,2,3), \tag{12}$$

where K_i and D_i $(i=1,2,3)$ are the thermal conductivity and diffusivity of the carbon layer, the ceramic layer, and the ceramic substrate, respectively; h is the heat transfer coefficient of the surface. R_{th} is the thermal boundary resistance between the ceramic grain layer and the substrate. L_1 and L_2 are the thicknesses of the carbon layer and the ceramic layer, respectively; α and R are the absorption coefficient and surface reflectivity of the carbon layer at the excitation wavelength, respectively, and P and a are the power and radius of the heating beam, respectively; $\omega=2\pi f$ is the angular modulation frequency. The surface temperature rise is determined by the contributions of direct heating and thermal diffusion, as well as accumulation/depletion (effective ''reflection'') at the interfaces and interference of the thermal wave. By measuring experimentally the amplitude and phase of the PTR signal as function of modulation frequency of the excitation beam, one can determine the thermal properties of different layers and the thermal impedances at interfaces.

The validation of the three-layer approximation for the grained ceramic sample depends on both the geometric structure (shape, orientation, mean size and distribution, etc.) of the grains and the size of the excitation beam. In ceramic samples with grain structure, there are thermal boundaries in all directions. To minimize the effect of lateral thermal barriers between grains on the transverse thermal conduction, a large excitation beam is preferable (compared to the lateral grain boundary-to-boundary distance) which produces a nearly uniform illumination near beam center (where the temperature rise is measured by an infrared detector in a PTR experiment) so there is essentially no thermal conduction across lateral vertical grain boundaries. In practice, any nonvertical lateral boundaries will contribute an effective projectional (horizontal) thermal impedance proportional to the mean impedance of the thermal boundary and the cosine of its inclination angle. This contribution becomes part of the effective forward thermal impedance measured photothermally in this work. The mean grain size must be comparable to the thermal diffusion length, defined as $L_{\text{th}}=\sqrt{D/\pi f}$, and this condition is expected to hold at the high-frequency end of the measurement. The thermal boundaries close to the surface can therefore be measured.

The thermal impedance at grain boundaries is represented in the three-layer model by a thermal boundary resistance R_{th}. The thermal resistance produces a temperature jump across the boundary. The thickness of the ceramic grain layer in the model represents a weighted thickness of the thermal barriers at all depths. The influence of thermal boundary resistance on the thermal conduction is accounted for by the parameter μ_2 [Eq. (10)], which decreases exponentially with the thickness L_2. Therefore thermal barriers close to the coated surface (the heat source) affect thermal conduction more strongly along the depth direction. Thermal boundaries deep inside the sample are also accounted for by the first boundary in the simple three-layer model, although their influence rapidly decreases with increasing depth. Because the theoretical model oversimplifies the complex ceramic grained sample to a simple three-layered sample, the

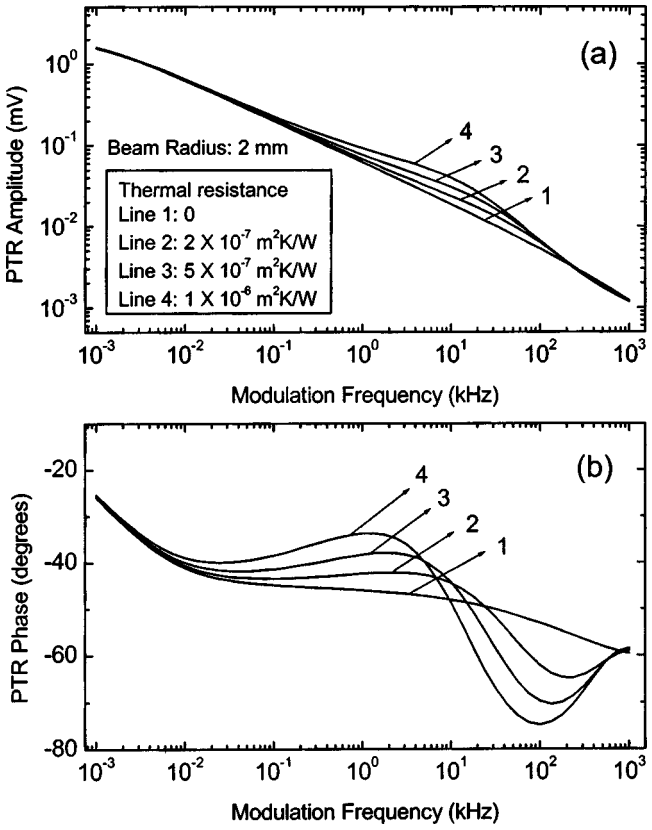

FIG. 2. Theoretical amplitude and phase of the PTR signal as a function of modulation frequency for a three-layered sample, showing the effect of thermal boundary resistance on the frequency behavior of the PTR signal.

value of the thermal boundary resistance R_{th} represents only a phenomenological (weighted) value of thermal resistance of boundaries at various depths, not the real value of the thermal resistance (expected to be variable) between ceramic grains.[20] However, the value of this approach lies in that a larger value of R_{th} certainly indicates a (overall) stronger thermal barrier between alumina grains.

III. THEORETICAL PREDICTIONS

In a PTR experiment, thermal infrared radiation from the sample surface is measured. The measured radiated power for the optically opaque geometry of Fig. 1 is given by the first-order approximation of the Stefan–Boltzmann law as

$$\Delta W(\omega) \approx 4\varepsilon\sigma T_0^3 \Delta T(z=0,\omega), \tag{13}$$

where σ is the Stefan–Boltzmann constant, ε is the surface emissivity, and T_0 is the ambient temperature. Equation (13) shows the PTR signal (the measured radiated power ΔW) is directly proportional to the surface temperature rise $\Delta T(z=0,\omega)$ caused by laser beam excitation.

The effect of thermal boundary resistance on the thermal wave transport in layered samples can be observed by the frequency dependence of the PTR signal. Figure 2 shows the effect of thermal resistance between ceramic layer and substrate on the amplitude and phase of the PTR signal as a function of the modulation frequency. The following parameters were used in the calculations: thermal conductivity, diffusivity and thickness of carbon over layer, respectively: 54 W/mK, 15 mm^2/s,[21] and 1 μm; of ceramic layer: 23.7 W/m K, 8.8 mm^2/s, and 2.4 μm. The heat transfer coefficient at the surface was assumed to be 200 $\mathrm{W/m}^2\,\mathrm{K}$.[21] The thermal conductivity and diffusivity of the ceramic substrate were the same as those of the ceramic layer. The radius of the excitation beam was 2 mm. The laser beam was assumed to be totally absorbed by the carbon layer. This was verified experimentally by observing the complete absence of transmitted pump-laser radiation leakage into the highly scattering ceramic substrate. The thermal boundary resistance affects both the amplitude and phase of the PTR signal in a wide frequency range, but most significantly when the thermal diffusion length is comparable to the thickness of the ceramic layer. Without thermal boundary resistance, the PTR amplitude decreases approximately inversely proportional to the square root of the modulation frequency (under one-dimensional condition) and the phase decreases from above $-45°$ to under $-45°$. At very low frequency, the effect of thermal resistance is negligible. At very high frequency the effect of thermal resistance is also diminished as the thermal wave cannot reach the thermal barrier. The thermal boundary resistance causes an increase of the amplitude in the intermediate frequency range, an increase of phase in the lower portion of the intermediate frequency range and a decrease of phase in the higher portion (a typical phenomenon of thermal-wave interference). The higher the thermal boundary resistance, the larger the amplitude increase and the larger the phase difference due to the increased confinement of the thermal-wave energy in the thin layer above the impedance boundary.

IV. EXPERIMENT AND MATERIALS

The experimental setup was described elsewhere.[16] In brief, a 514.5 nm wavelength continuous wave Ar^+ laser from Coherent was modulated by an external acousto-optic modulator (ISOMET 1201E-1) and then focused by a focusing lens onto the sample surface. The beam size was adjustable between 0.5 and 5 mm by changing the position of the focusing lens. The blackbody radiation from the optically excited sample was collected and collimated by two off-axis paraboloidal reflectors and then focused onto a liquid-nitrogen-cooled HgCdTe (mercury–cadmium–telluride) detector (EG&G Judson Model J15D12-M204-S01M). An anti-reflection-coated germanium window with a transmission bandwidth of 2–14 μm was mounted in front of the detector to block any visible synchronous radiation from the pump laser. The detected PTR signal was sent to a lock-in amplifier (EG&G Princeton Applied Research Model 5210) and recorded on a personal computer (PC). The process of data acquisition, storage, and frequency scanning was fully automated via the PC. Both amplitude and phase of the PTR signal were recorded as a function of modulation frequency ranging from 10 Hz to 100 kHz.

Three ceramic samples were used in the measurements: one original ceramic sample labeled as 01 and two ASPRO treated samples labeled as 1 and 2, treated under different conditions 1 and 2, respectively (see below). All samples consisted of cylindrical sections of 4.75 mm thickness, 3.85

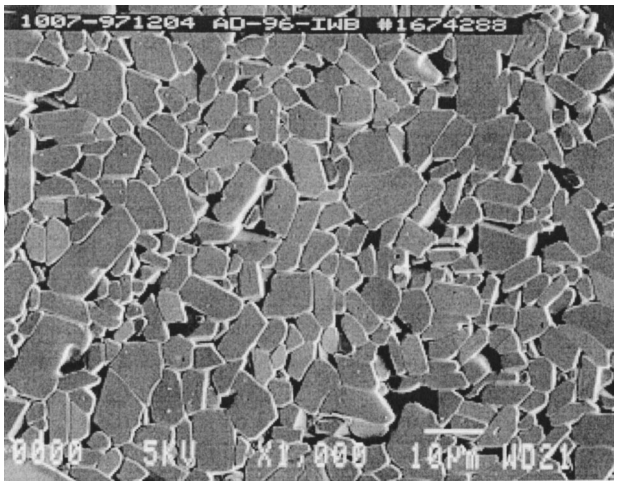

FIG. 3. Microstructure of the untreated alumina sample.

cm internal radius and 4.13 cm outer radius. The lateral size of all samples was $20\times25\ \mathrm{mm}^2$. The original alumina samples used as ceramic cylinder liners were prepared in CoorsTek, Inc. (CO) and the ceramic material was marked as AD-96. The calcined alumina powder was milled and mixed with mineralizing agents to introduce grain growth inhibitors plus fluxing additives to tailor the body formulation to the firing conditions. The alumina cylinder samples were prepared by cold isostatic pressing of spray-dried powder under 138 MPa and then sintered at 1600 °C to the full density in a natural gas fired tunnel kiln. After firing, the liquid dye penetrant immersion was used to ensure that the ceramic samples had been fired to full density and there was no residual porosity and, at the same time, to make sure there were no cracks. The sintered ceramic cylinders were machined by diamond grinding to the final inside diameter/outside diameter tolerances. The chemical composition of the ceramic sample was 96% alumina, ~3% silica, ~0.9% MgO, and less significant amounts of other oxides. The entire ceramic liners were additionally treated by the ASPRO conversion technology, introduced at ATS Spartec–AHCS, Inc. for treating finished ceramic components.[3] The ASPRO process can modify ceramic properties by varying the applied pressure and temperature. During that process ceramic samples were subjected to a range of temperature and pressure treatment, with a maximum applied temperature of ~1000 °C and pressure of ~2.8 GPa. The maximum applied temperatures were ~1000 and 800 °C for treated samples 1 and 2, respectively. The resulting ceramic samples have nearly full density with high thermal shock resistance, while maintaining a unique combination of desired properties, such as high levels of toughness, hardness, chemical and wear resistances.[2,22] The ceramics consisted of alumina grains embedded in a second (glass) phase, the main composition of which is silica, in addition to alumina phase and minor amounts of MgO and CaO. The thickness range of the second phase boundaries is estimated to be 0–3 μm. In ceramic materials, the boundaries between grains have a large, often controlling, importance to the mechanical, thermal, and electrical properties. The mean size of alumina grains was 6 μm. Figure 3 shows the microstructure of an untreated sample cross section, exhibiting a relatively uniform grain shape and size. After the ASPRO treatment, no noticeable changes in the microstructure of the sample were observed. The appropriate mean grain size justifies the validation of the three-layered model, as discussed in Sec. II.

The mechanical and thermal properties of alumina ceramics before and after ASPRO treatment were measured

TABLE I. Properties of original and ASPRO-treated alumina ceramics (see Ref. 22) (96% Al_2O_3/3% SiO_2/0.9% MgO).

Properties	Units	01 Untreated alumina	1 ASPRO treated alumina	Measurement uncertainty
Density, 20 °C	g/cm^3	3.712	3.716	±0.1%
Elastic modulus, 20 °C	GPa	320	319	±0.5%
Poisson's ratio		0.216	0.217	±0.5%
Hardness	GPa	12.1	12.3	±3.3%
Fracture toughness	MPa m	4.0	3.4	±20%
Thermal shock resistance, ΔTc	°C	<300	>650	
Thermal expansion coefficient	1×10^{-6}/°C			±3–5%
35–300 °C		7.36	7.15	
300–500 °C		8.05	6.94	
500–800 °C		8.71	8.54	
Thermal conductivity	W/m K			±4%–5%
20 °C		23.7	21.5	±1–2 W/m K
100 °C		18.9	17.6	
200 °C		15.0	14.4	
300 °C		12.5	12.2	
Specific heat	J/kg K			±2.5%
20 °C		724.7	712.3	
100 °C		871.1	868.0	
200 °C		989.5	986.5	
300 °C		1065	1070	

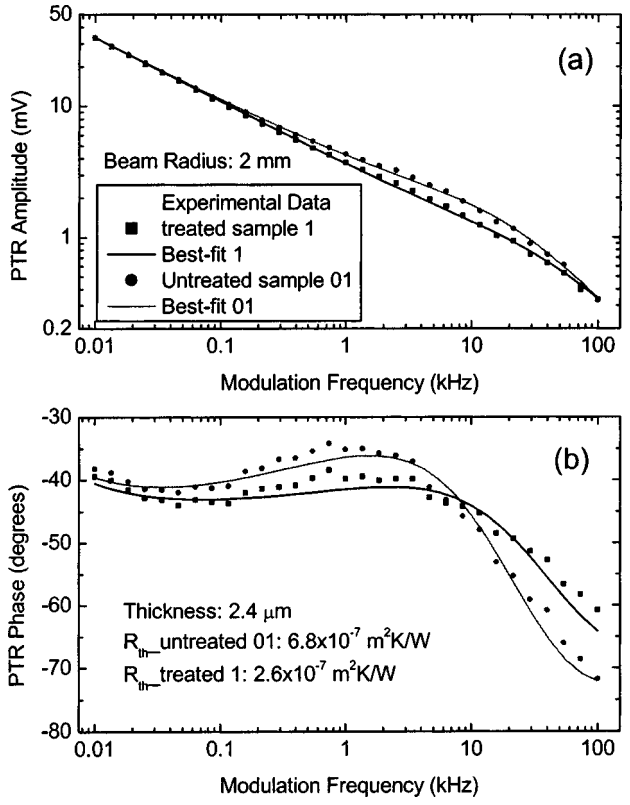

FIG. 4. Measurements on untreated 01 and treated 1 samples and the best fits. The fits give thermal resistance of 6.8×10^{-7} W/m^2 K for the untreated (01) sample and 2.6×10^{-7} W/m^2 K for the treated (1) sample.

and the results are presented in Table I. There were no significant differences (within measurement error) between both mechanical and thermal properties of the original and ASPRO-treated ceramics, except for the thermal shock resistance. The ASPRO treatment significantly improved the thermal shock resistance of the alumina ceramics used in this work. Its value was increased from the critical temperature differences, ΔT_c (between sample surface and quenching media), of less than 300 °C to more than 650 °C, as measured by rapid heating using melted aluminum.[3,22] Successful experimental trials of the treated alumina liners in an oxygen gas flame, and manufactured internal combustion engines and castings of molten aluminum have previously validated the effectiveness of the treatment in withstanding extreme thermal shock.[2,22]

The PTR measurements were performed on the coated surfaces of the ceramic samples with an estimated carbon coating thickness of 1 μm. In all measurements, the power of the Ar ion laser was approximately 25 mW and the beam radius was approximately 2 mm.

V. EXPERIMENTAL RESULTS

All samples were measured under the same conditions at room temperature. Figure 4 shows typical results of the measurements for the untreated (01) and a treated (1) sample. The experimental data were fitted with the theoretical model via a multi-parameter fitting procedure and the best- fit curves are also shown in the figure. In the multi-parameter fitting procedure, the thermal properties and thickness of the carbon were assumed to be known and were the same as those used in Fig. 2. The thermal conductivity and diffusivity of the alumina ceramic were assumed to be 23.7 W/m K and 8.8 mm^2/s, respectively, measured independently on the untreated sample (see Table I). The heat transfer coefficient at the surface was assumed to be 200 W/m^2 K[21] (the fitting results were relatively insensitive to variation of h from 0 to 2000 W/m^2 K). Both amplitude and phase of the PTR signal were used in the multi-parameter fitting and the following square variance was minimized via a least squares procedure

$$\mathrm{var}=e\cdot\frac{\Sigma_{m=1}^{N}\{\ln[A^T(f_m)]-\ln[A^E(f_m)]\}^2}{\Sigma_{m=1}^{N}\{\ln[A^E(f_m)]\}^2}+\frac{\Sigma_{m=1}^{N}[\Phi^T(f_m)-\Phi^E(f_m)]^2}{\Sigma_{m=1}^{N}[\Phi^E(f_m)]}. \quad (14)$$

Here $A^T(f_m)$ and $\Phi^T(f_m)$ are the theoretical amplitude and phase of the PTR signal and $A^E(f_m)$ and $\Phi^E(f_m)$ are the experimental amplitude and phase at modulation frequency f_m, respectively. The logarithm of the amplitude instead of the amplitude itself was used in the variance function because of the strong attenuation of amplitude with modulation frequency (see Fig. 2). A typical mean square variance for the logarithm of amplitude was between 0.0001 and 0.0002 and for the phase was between 0.0008 and 0.0013, with a total mean square variance less than 0.0015.

In the multi-parameter fitting, both the ceramic layer thickness and the thermal boundary resistance were first set as free parameters for both untreated and treated samples. To compare directly and quantitatively the thermal boundary resistance of the untreated and treated ceramic samples, the ceramic layer thickness was then fixed to the average of the fitted thickness values for both samples. In general, the fitted thicknesses for the untreated and treated samples were close to each other. For example, the fitted thickness was 2.5 μm for the untreated sample 01 and 2.4 μm for the treated sample 1. For the treated sample 2 (not shown in Fig. 4), the fitted thickness was also 2.4 μm. With the same ceramic layer thickness of 2.4 μm, the fitted thermal boundary resistance was 6.8×10^{-7} m^2 K/W for the untreated 01 sample. After the ASPRO treatment, the thermal resistance was reduced to 2.6×10^{-7} m^2 K/W for both treated samples 1 and 2. Measurement results show that in all cases the treated samples exhibited lower thermal boundary resistance than the untreated samples, regardless of the conditions of treatment. Because the surface of the ceramic samples was ground during preparation, the depths of grains close to the surface varied from very thin (less than 1 μm) to over the mean size of the grains, with an average depth of roughly 3.0 μm, a half of the mean size. The fitted thickness of the ceramic layer, 2.4 μm, was close to the average depth, 3.0 μm, as expected.

From Fig. 4 the agreement between experimental measurements and theoretical predictions is good, considering the theoretical model is oversimplified. The goodness of fits is also indicated by the low mean square variance (the variance value is 0.0014 for the untreated sample 01 and 0.0015 for the treated sample 1). The phase discrepancy at the low-frequency range may possibly be caused by lateral thermal

barriers. At low frequency the thermal diffusion length is comparable to the beam size. Lateral thermal conduction is not negligible and is affected by the lateral thermal boundaries. It is well known[23] that higher-dimensional thermal-wave transport affects the signal phase more sensitively than the amplitude. For this reason, the theoretical amplitude in Fig. 4(a) appears to be much better fitted to the data than the phase in Fig. 4(b). Another reason for the low-frequency phase mismatch may be thermal barriers present deep in the sample which were not accounted for in the model: those would have required a multilayer model. Even though the fitted values of thermal boundary resistance do not quantitatively represent the thermal resistance at ceramic grain boundaries, these values do give a qualitative comparison between the untreated and the treated samples. A higher thermal boundary resistance value fitted with the three-layer model, in principle, indicates a higher thermal resistance at the ceramic grain boundaries. The measurement results indicate that the ASPRO treatment significantly reduced the thermal resistance between alumina grains.

In an attempt to theoretically take into account the heterogeneous structure of the grained ceramic sample, a multilayer model[19] (up to ten layers were assumed) was tried to approximately describe the grain boundary structure (see Fig. 3) in the depth direction. It turned out that the three-layer model adequately carries the major features of the multilayer model at considerable simplification, due to the fact that thermal resistances at boundaries closer to the modulated thermal source (the coated surface) affect the thermal wave propagation more strongly (see Sec. II). On the other hand, the effect of lateral grain boundaries on the thermal conduction is negligible, as discussed in detail in Sec. II, due to the fact that an excitation beam the size of which is much larger than the lateral boundary-to-boundary distance was used in the experiment and the thermal conduction is therefore essentially one dimensional (depth direction). The three-layer model was therefore found adequate to yield a phenomenological (effective) value of the inter-grain thermal impedance, as witnessed by the simulations and the fits to the experimental data.

It is worth noting that the PTR amplitudes for both untreated and treated ceramic samples were close to each other at the low- and high-frequency ends. This indicates that the effective thermal conductivities of both samples are very close, due to the fact that PTR amplitude at the low- or high-frequency end is approximately inversely proportional to the effective thermal conductivity of the samples under instigation. The thermal conductivity was not set as a free parameter in the multi-parameter fitting, as we had independent measurements of that parameter and the three-layer model oversimplified the actual condition of the complex grained ceramic samples. However, if the thermal conductivity (K) was set as a free parameter along with the thickness and the thermal boundary resistance, the fitted K values for the untreated and treated samples were very close to each other and lay between the independently measured effective K value of the ceramic sample and the literature K value of the alumina crystal.[24] Independent measurements performed under steady state conditions showed that the thermal conductivity of the treated ceramic sample was slightly lower than that of the untreated sample (see Table I). However, this difference is not significant considering a measurement error of 1–2 W/mK. The measured effective thermal conductivity was close to the theoretical value of a composite consisting of 96% alumina, 3% silica, and 1% MgO, assuming perfect thermal contact at grain boundaries.[25–27] These results suggest that thermal resistance at grain boundaries is relatively small and its effect to steady state thermal conduction is negligible, while under transient conditions such as in thermal shock experiments these thermal barriers affect the thermal conduction significantly. This point is well explained by the results presented in Fig. 2. The thermal boundary resistance significantly affects the frequency behavior of the PTR signal only when the modulation frequency is higher than a characteristic frequency which depends on the magnitude of thermal boundary resistance and the thermal properties of the material.[19] Under one-dimensional heat transport, the effect of thermal resistance R_{th} on the thermal conduction becomes significant when R_{th} is comparable to L_{th}/K, with L_{th} the thermal diffusion length and K the thermal conductivity of the ceramic layer.

It should be pointed out that thermal interfacial resistance at grain boundaries may reduce the effective thermal conductivities of the grained ceramic materials, depending on the magnitude of the resistance.[25–27] In principle the effect of the thermal boundary resistance could be estimated by directly comparing the effective thermal conductivities of the ceramic samples before and after ASPRO treatment.[28] However, independent measurement under steady state conditions on the effective thermal conductivities of ceramic samples with and without ASPRO treatment showed that the thermal conductivity of the treated sample was close to, or even slightly lower than, that of the untreated sample, thus indicating that the influence of the thermal boundary resistance on the effective thermal conductivity is negligible under *steady state* conditions. Yet its influence under *transient* conditions, such as thermal-wave probing and as occurring in thermal shock experiments is significant and as discussed above. Furthermore, simulation results showed that the unique difference in the frequency behavior of untreated and ASPRO-treated samples as presented in Fig. 4, which is well above the measurement error, could not be explained and fitted by any other combination of thermal parameter changes other than the inter-grain thermal impedance. The good agreement between experimental data and theoretical fits (see Fig. 4) unambiguously proves that the presence of an inter-grain boundary impedance controls the thermal shock behavior of the alumina ceramics, as discussed below.

VI. DISCUSSION

Thermal shock tests performed with both untreated and treated ceramic samples showed that the ASPRO treatment significantly improves the thermal shock resistance of the alumina ceramic material by a factor of >2.1, from the critical temperature differences (ΔT_c) of less than 300 to over 650 °C.[22] The thermal shock resistance is a measure of the maximum temperature difference that a material can with-

stand without catastrophic failure. In a thermal shock experiment, a transient thermal load is applied to the sample surface by melted aluminum and a high temperature flame heating,[22,29] or transient cooling is applied by quenching if the sample is initially heated to an elevated temperature,[30] which produces a large temperature gradient inside the sample and therefore a strong thermal stress. Once the thermal stress exceeds a threshold determined by the mechanical and thermal properties of the sample, catastrophic failure occurs.

The PTR measurement results presented in Sec. V indicated that the ASPRO-treated ceramic samples had lower thermal resistance at grain boundaries than the untreated samples. These results show that the ASPRO treatment reduces the thermal resistance between alumina grains in the ceramic sample, and thus decreases the thermal gradient across the inter-grain region. Therefore it reduces the local thermal stress there, which results in an improvement of the thermal shock resistance.[30]

A thermal boundary resistance R_{th} is defined in terms of a temperature jump ΔT, that occurs across the boundary, in response to a heat flux Q, in a direction normal to the interface

$$R_{\mathrm{th}}=\frac{\Delta T}{Q}. \tag{15}$$

Equation (15) indicates that the temperature gradient across the boundary is directly proportional to the thermal boundary resistance. The thermal stress caused by a temperature gradient in a material is expressed as follows:[30]

$$\sigma=\frac{E\alpha_T\Delta T}{(1-\nu)}, \tag{16}$$

where σ is the thermal stress, α_T is the coefficient of linear thermal expansion, ν is Poisson's ratio, and ΔT is the temperature gradient. Once the temperature-gradient-induced thermal stress exceeds the tensile strength of the material, the sample will fail catastrophically. From Eqs. (15) and (16) it is apparent that a lower thermal resistance at the grain boundaries would result in a higher thermal shock resistance.

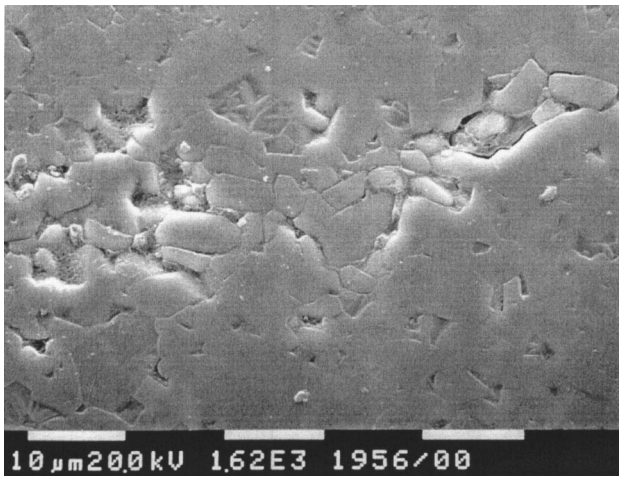

FIG. 5. Microstructure of the treated ceramic sample showing crack paths.

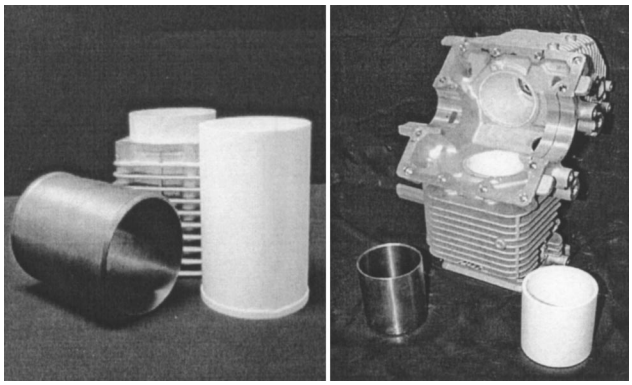

FIG. 6. Components of the internal combustion blocks with the ASPRO-treated alumina ceramic liners: motorcycle engine components (left) and overhead cam twin engine components (right).

By reducing the thermal resistance at the inter-grain region, the ASPRO treatment improves the thermal shock behavior of the ceramic sample. For grained ceramic samples investigated in this experiment, the thermal-shock-induced crack paths should follow grain boundaries, since these are the loci of the maximum temperature gradient. This has been confirmed by microscopic observation of a cross section of our alumina ceramics as shown in Fig. 5. Another observation which supports the thermal boundary resistance explanation is that the thermal shock resistance of alumina samples becomes significantly higher if the material is put under compression. Compression improves the thermal contact between alumina grains, thereby reducing the thermal boundary resistance and resulting in a higher thermal shock resistance. The improved thermal transport properties of the ASPRO-treated ceramic materials appear to be well suited for applications in internal combustion engines. This type of alumina cylinder liner has been successfully installed and tested in different internal combustion engines (Fig. 6).[2,22]

VII. CONCLUSIONS

The photothermal radiometric technique has been used to measure the thermal properties of alumina ceramic materials treated by a specific temperature-pressure process (ASPRO).[2,22] Alumina ceramics with ASPRO treatment have exhibited much higher thermal shock resistance than corresponding untreated ceramics. The excellent agreement of the experimental results to the three-layered thermal-wave theoretical model of Sec. II indicates that the thermal behavior of these samples is consistent with the presence of an inter-grain thermal boundary impedance which controls the thermal shock behavior of the ceramics. This improvement in thermal shock behavior was found to be the result of the reduction of thermal resistance between ceramic grain boundaries, as measured by the PTR technique, without a concomitant change in the thermal conductivity of the material.

ACKNOWLEDGMENTS

The support of Materials and Manufacturing Ontario (MMO) with an Interact contract and of the National Research Council of Canada-IRAP (NRC-IRAP) is gratefully acknowledged.

[1] H. Wang and R. N. Singh, Int. Mater. Rev. **39**, 228 (1994).
[2] Z. Z. Kish, Sixth International Conference on Coatings for Aerospace and Automotive Industries, Toronto, Canada, 20–22 October, 1999, pp. 39A and 39B
[3] A. Hansma, US Patent, No. 65,44,458 (8 April 2003).
[4] *Progress in Photothermal and Photoacoustic Science and Technology*, edited by A. Mandelis (Elsevier, New York, 1992), Vol. I.
[5] J. Hartmann, M. Costello, and M. Reichling, Phys. Rev. Lett. **80**, 117 (1998).
[6] J. C. Murphy and L. C. Aamodt, Appl. Phys. Lett. **39**, 519 (1981).
[7] L. J. Inglehart, J. Appl. Phys. **68**, 2992 (1990).
[8] A. Sanchez-Lavega, A. Salazar, A. Ocariz, L. Pottier, E. Gomez, L. M. Villar, and E. Macho, Appl. Phys. A: Mater. Sci. Process. **65**, 15 (1997).
[9] B. Li, L. Pottier, J. P. Roger, D. Fournier, K. Watari, and K. Hirao, J. Eur. Ceram. Soc. **19**, 1631 (1999).
[10] J.-F. Bisson and D. Fournier, J. Am. Ceram. Soc. **83**, 1993 (2000).
[11] K. R. McDonald, J. R. Dryden, and F. W. Zok, J. Am. Ceram. Soc. **84**, 2015 (2001).
[12] L. Wei and G. S. White, J. Mater. Res. **12**, 2381 (1997).
[13] T. T. N. Lan, U. Seidel, and H. G. Walther, J. Appl. Phys. **78**, 4108 (1995).
[14] K. R. McDonald, J. R. Dryden, A. Majumdar, and F. W. Zok, J. Heat Transfer **122**, 10 (2000).
[15] P. E. Nordal and S. O. Kanstad, Phys. Scr. **20**, 659 (1979).
[16] L. Nicolaides, A. Mandelis, and C. J. Beingessner, J. Appl. Phys. **89**, 7879 (2001).
[17] A. Salnick, A. Mandelis, and C. Jean, Appl. Phys. Lett. **69**, 2522 (1996).
[18] L. Nicolaides, A. Mandelis, and S. H. Abrams, J. Biomed. Opt. **5**, 31 (2000).
[19] B.-C. Li and S. Y. Zhang, J. Phys. D **30**, 1447 (1997).
[20] D. S. Smith, S. Fayette, S. Grandjean, and C. Martin, J. Am. Ceram. Soc. **86**, 105 (2003).
[21] Y.-C. Yang, W.-J. Chang, and H.-L. Lee, J. Appl. Phys. **88**, 6987 (2000).
[22] Z. Z. Kish, *Developments of High Performance Alumina Ceramics for Engine Components*, ATS Spartec–AHCS, Inc., 2002 (unpublished).
[23] A. Mandelis, *Diffusion-Wave Fields: Mathematical Methods and Green Functions* (Springer, New York, 2001), Chap. 4.
[24] C. L. Yaws, *Handbook of Thermal Conductivity* (Gulf Pub., Houston, 1995).
[25] D. P. H. Hasselman and L. F. Johnson, J. Compos. Mater. **21**, 508 (1987).
[26] C.-W. Nan, R. Birringer, D. R. Clarke, and H. Gleiter, J. Appl. Phys. **81**, 6692 (1997).
[27] M. I. K. Collin and D. J. Rowcliffe, J. Am. Ceram. Soc. **84**, 1334 (2001).
[28] C.-W. Nan, X.-P. Li, and R. Birringer, J. Am. Ceram. Soc. **83**, 848 (2000).
[29] P. K. Panda, T. S. Kannan, J. Dubois, C. Olagnon, and G. Fantozzi, J. Eur. Ceram. Soc. **22**, 2187 (2002).
[30] A. P. Bayuseno, B. A. Latella, and B. H. O'Connor, J. Am. Ceram. Soc. **82**, 819 (1999).